

Zeeman effect in oscillations of magnetars with toroidal magnetic fields

D. G. Yakovlev*

Ioffe Institute, Politekhnikeskaya street 26, Saint Petersburg, 194021, Russia

I. E. Fedorov

Murino Educational Center Nr. 2, Mendeleev boulevard 20/1, Murino, Leningrad region, 188662, Russia

(Dated: November 28, 2024)

Magnetars are neutron stars with superstrong magnetic fields. Some of them (soft-gamma repeaters, SGRs) demonstrate gigantic flares which nature is still unclear. At decay phase of such flares one often observes quasi-periodic oscillations (QPOs) which are treated as stellar oscillations triggered by the flares. We study, for the first time, magneto-elastic oscillations of magnetars possessing toroidal magnetic fields confined in the stellar crust, without imposing axial symmetry of perturbations. We show that the Zeeman effect makes the oscillation spectrum much richer than for axially symmetric oscillations. The main properties of theoretical QPO spectra are discussed as well as their potential to interpret observations and explore magnetar physics.

PACS numbers: 97.60.Jd, 04.40.Dg, 98.70.Rz, 32.60.+i

I. INTRODUCTION

Zeeman splitting of quantum energy levels by a magnetic field is a famous physical effect. It is remarkable that it can be observed on macrophysical level in such exotic objects as magnetars which are neutron stars with superstrong magnetic fields. The Zeeman effect can split oscillation frequencies of magnetars which is useful for exploring basic properties of these objects.

Neutron stars attract great attention because they contain matter under extreme physical conditions; many properties of this matter are still not clear (e.g. Refs. [1, 2]). Generally, neutron stars consist of two main layers: the outer layer often called the crust, and the core. For a typical neutron star with the mass $M \sim 1.4 M_{\odot}$ (M_{\odot} being the solar mass) the radius is $R \sim 12$ km. The crustal matter consist mainly of ions (atomic nuclei), electrons and (at densities $\rho \gtrsim 4 \times 10^{11}$ g cm $^{-3}$) free neutrons. The crust depth is ~ 1 km, and its mass is $\sim 0.01 M_{\odot}$. At the crust bottom the density reaches about one half of the saturation density of nuclear matter (the latter being about $\rho_0 \approx 2.8 \times 10^{14}$ g cm $^{-3}$). As a rule, atomic nuclei in the crust form Coulomb crystal. Under the crust, there is a bulky and massive core containing superdense nuclear matter. The central density reaches several ρ_0 .

Magnetars form a special class of neutron stars (see Ref. [3] for a comprehensive review). Many problems of their structure and evolution are still under debates employing rather controversial models, although it is generally believed that the presence of strong magnetic fields is crucial. We will be interested in an important group of magnetars called soft-gamma repeaters (SGRs). Occasionally they demonstrate extremely powerful flares (with total energy release up to $\sim 10^{46}$ erg). At the decay

phase of these flares one often detects quasi-periodic oscillations (QPOs) of X-ray and soft gamma-ray emission with typical frequencies from a few tens Hz to several kHz.

Neither the mechanism of triggering the flares nor the mechanism of QPO generation are known, and we will not study them here. Nevertheless, it is commonly thought that the flares are regulated by strong magnetic fields (e.g. Ref. [3]), and the QPOs are associated with oscillations of magnetars excited in the flares.

The QPOs were theoretically predicted in Ref. [4]. They were discovered [5–7] in 2005–2006 after processing the observations of the giant flare of SGR 1900+14 (27/09/1998) and the hyperflare of SGR 1806–20 (27/12/2004). These observations, as well later observations of other SGRs, have been processed and reprocessed (e.g., [8–11]).

Magnetar QPOs are usually treated as torsional neutron star pulsations associated with sufficiently slow elastic shear perturbations in crystallized crust and/or Alfvén perturbations due to elasticity of magnetic field lines. Their typical propagation speeds are, respectively, the shear and Alfvén velocities. Shear perturbations exist in the crystallized crust, but Alfvén perturbations are not necessarily confined there: they can propagate to other magnetized regions of stars. In the absence of magnetic field, they are purely torsional shear modes. In the presence of the field, they are called torsional magneto-elastic, or just magneto-elastic modes. In very high fields crystal elasticity may become unimportant.

The theory of torsion shear oscillations was began in 1980s [12–14]. It was further elaborated after the discovery of QPOs; see, e.g. Refs. [15–26], simultaneously with rapidly developing theory of magneto-elastic oscillations; e.g. Refs. [27–47]. The latter publications have been mostly restricted to studying axially symmetric magnetic fields and deformations of fluid elements. These studies neglected Zeeman splitting of oscillation frequencies by magnetic fields which made the family of theoretical fre-

* yak.astro@mail.ioffe.ru

quencies incomplete.

The Zeeman splitting of magnetar QPOs was first discussed and properly estimated by Shaisultanov and Eichler [48] in 2009, but their publication did not attract much attention. Two other publications [49, 50] on the subject, devoted to magnetars with dipole magnetic fields in the crust, appeared only recently. They demonstrated, using the first-order perturbation theory with respect to magnetic field strength, that the Zeeman effect greatly enriches the QPO spectrum and strongly affects QPO interpretation.

Here we use the same formalism for studying the combination of axially symmetric poloidal and toroidal fields (Sec. II), and apply the results to the case of purely toroidal fields (Sec. III). The latter case is simpler and can be done with more confidence. We discuss the relation of new theoretical results to observations in Sec. IV and conclude in Sec. V.

II. THEORY

A. General remarks

Since the standard formalism for studying magneto-elastic oscillations in magnetars is well known (e.g., [38, 39]), we describe it briefly. A non-oscillating star is assumed to possess a stationary magnetic field $\mathbf{B}(\mathbf{r})$ which is not too strong ($\lesssim 5 \times 10^{15}$ G) to violate global stellar sphericity. The oscillations are thought to be small, and treated in the linear approximation as non-dissipative motion of incompressible matter and magnetic field perturbations frozen into that matter. In this case, local matter elements move along respective spherical surfaces and produce neither perturbations of the pressure nor generation of gravitational waves. We focus on the perturbations located mostly in the magnetar crust.

According to calculations (e.g., [25]), the most important place for driving the crustal oscillations is the layer near the crust bottom, at $\rho \sim 10^{14}$ g cm $^{-3}$. A characteristic estimate of the shear velocity there, defined by the shear modulus μ of the crystal, is $v_\mu \sim \sqrt{\mu/\rho} \sim 10^8$ cm s $^{-1}$. A typical estimate of the Alfvén velocity gives $v_A = B/\sqrt{4\pi\rho} \sim 3 \times 10^7 B_*$ cm s $^{-1}$, where B_* is the magnetic field in units of 10^{15} G. The velocities v_μ and v_A become comparable at $B \sim B_\mu \sim 3 \times 10^{15}$ G. This is a characteristic field strength which separates two regimes in which the oscillations are mainly determined by shear effects ($B \lesssim B_\mu$) and Alfvén waves ($B \gtrsim B_\mu$). As demonstrated below, for high oscillation frequencies B_μ becomes lower.

B. Reference frames

We will use three different reference frames.

Firstly, we can employ the standard Newtonian approach in spherical coordinates (r, θ, ϕ) . It is simple and clear.

Secondly, we can describe the neutron star crust in full General Relativity (GR) with the metric

$$ds^2 = -c^2 e^{2\Phi} dt^2 + e^{2\Lambda} dr^2 + r^2(d\theta^2 + \sin^2\theta d\phi^2), \quad (1)$$

where t is Schwarzschild time (for a distant observer), r is circumferential radius, θ and ϕ are ordinary spherical angles, while $\Phi(r)$ and $\Lambda(r)$ are two metric functions determined by solving the standard GR equations for a spherical star (e.g., Ref. [2]).

Thirdly, taking into account that the crust is thin and low-massive, we can also use a simplified GR description with the metric (1), where Φ and Λ are taken constant,

$$\Lambda = -\Phi, \quad e^\Phi = \sqrt{1 - x_g}. \quad (2)$$

Here $x_g = 2GM/(c^2R)$ is the neutron star compactness parameter, G is the gravitational constant, c is the velocity of light, while M and R are the gravitational stellar mass and circumferential radius, respectively.

This approximation is well known in neutron-star physics; it has been used for studying various problems of structure and evolution of the crust (e.g., Ref. [2]). It allows one to introduce a local crustal reference frame, which is nearly flat, and then solve corresponding Newtonian problem in that frame. For comparing with full GR, one should transform the results for a distant observer.

Note, that dr in GR is a proper measure of circumferential distances, while proper distances in radial direction are measured by $d\tilde{r} = e^\Lambda dr$. Then, while using the simplified GR description after starting from Newtonian equations in the crustal reference frame, it would be better to treat radial derivatives of any function f (designed formally as $\partial f/\partial r$) in a Newtonian solution as $\partial f/\partial \tilde{r} \rightarrow e^{-\Lambda} \partial f/\partial r$, keeping r for measuring circumferential distances. Note also that if $\tilde{\omega}$ is an oscillation frequency in the crustal frame, then a distant observer detects the redshifted frequency $\omega = \sqrt{1 - x_g} \tilde{\omega}$.

C. Standard equations

To outline the equations which govern magneto-elastic oscillations, we follow Refs. [49, 50] and disregard temporarily the GR effects using the Newtonian approach.

The oscillations excite small velocities of matter elements $\mathbf{v}(\mathbf{r}, t)$, small displacements of these elements $\mathbf{u}(\mathbf{r}, t)$, and small variations of magnetic fields $\mathbf{B}_1(\mathbf{r}, t)$. All these quantities oscillate as $e^{i\omega t}$, where ω is the angular oscillation frequency. This overall oscillating factor in the linearized oscillation equations can be dropped, leading to the stationary wave equation for small (generally complex) amplitudes $\mathbf{u}(\mathbf{r})$ and $\mathbf{B}_1(\mathbf{r})$, and for ω :

$$\rho_H \omega^2 \mathbf{u} = \mathbf{T}_\mu + \mathbf{T}_B. \quad (3)$$

Here $\rho_H = \rho + P/c^2$ is the enthalpy density of neutron star matter, a proper measure of inertial mass density, determined by the real mass (energy) density ρ and by the pressure P . Furthermore, \mathbf{T}_μ and \mathbf{T}_B are the mean volumetric densities of forces (with minus sign) determined, respectively, by the crystal elasticity and Alfvén perturbations. In the case of elasticity

$$T_{\mu i} = -\frac{\partial \sigma_{ik}}{\partial x_k}, \quad \sigma_{ik} = \mu \left(\frac{\partial u_i}{\partial x_k} + \frac{\partial u_k}{\partial x_i} \right), \quad (4)$$

σ_{ik} being the tensor of shear deformations and μ the shear modulus in the isotropic-crystal approximation. In the case of magnetic forces,

$$\mathbf{T}_B = \frac{1}{4\pi} \mathbf{B} \times \text{curl } \mathbf{B}_1, \quad \mathbf{B}_1 = \text{curl}(\mathbf{u} \times \mathbf{B}). \quad (5)$$

The equations should be supplemented with boundary conditions. Since local matter elements move along respective spheres, the crust-core interface remains spherical. Generally, Alfvén perturbations can propagate outside the crust, and one needs additional dynamical equations in the outside magnetized regions with corresponding outside boundary conditions. In Secs. D and E we argue that our restricted problem can be studied by solving dynamical equations in the crust and by requiring the radial components of shear stresses to vanish at crust boundaries.

D. Case of $\mathbf{B} = 0$

This case has been solved in full GR (e.g., [13, 29]), and we discuss these solutions. Any stationary wave function $\mathbf{u}(\mathbf{r})$ has two non-trivial components, u_ϕ and u_θ (since $u_r = 0$).

It is instructive to introduce the full set of basic wave functions for torsion oscillations at $\mathbf{B} = 0$ (e.g., [49]). They can be specified by the three quantum numbers (n, ℓ, m) , where $n = 0, 1, 2, \dots$ is the number of radial nodes, ℓ is the orbital quantum number which runs in integer values $\ell \geq 2$ in the given problem, and m is the azimuthal quantum number running integer values from $-\ell$ to ℓ . The basic wave functions read

$$u_\phi(r, \theta, \phi) = rY(r) e^{im\phi} \frac{dP_\ell^m}{d\theta}, \quad (6)$$

$$u_\theta(r, \theta, \phi) = rY(r) e^{im\phi} \frac{imP_\ell^m}{\sin \theta}, \quad (7)$$

where r is the circumferential radius, $P_\ell^m(\cos \theta)$ is an associated Legendre polynomial (e.g., Ref. [51]), and $Y(r) = Y_{n\ell}(r)$ is a radial wave function obeying the equation

$$Y_{,rr} + \left(\frac{4}{r} + \Phi_{,r} - \Lambda_{,r} + \frac{\mu_{,r}}{\mu} \right) Y_{,r} + \left[\frac{\rho_H}{\mu} e^{-2\Phi} \omega_\mu^2 - \frac{(\ell+2)(\ell-1)}{r^2} \right] e^{2\Lambda} Y = 0. \quad (8)$$

The symbols $,r$ and $,rr$ in the subscripts mean derivatives over r . The frequencies of such pulsations are denoted as ω_μ .

These oscillations are locked in the crystalline crust, $R_1 \leq r \leq R_2$, where R_1 labels the boundary between the crust and the liquid stellar core, while R_2 labels the outer boundary of the crystal, that is very close to the stellar radius R . At both boundaries the radial shear stresses should vanish: $Y_{,r}(R_1) = Y_{,r}(R_2) = 0$. Such oscillations are degenerate in m : $\omega_\mu = \omega_{\mu n \ell}$ and $Y = Y_{n\ell}(r)$ are independent of m . The boundary value $Y_0 = Y(R_2)$ characterizes the angular amplitude of oscillations (in radians) of the outer boundary of the crystal. If $m = 0$, crystalline matter oscillates along respective circles ($u_\theta = 0$, at constant r and θ); meridional motions appear at $m \neq 0$. Any specific stellar model affects only $Y(r)$; the angular dependence of $\mathbf{u}(\mathbf{r})$ stays standard.

It is important that oscillation frequencies ω_μ can be expressed as ratios of integrals over the crystallized matter [13] (also see, e.g., [25, 26]):

$$\omega_\mu^2 = \frac{\int dV \mu [r^2 e^{\Phi-\Lambda} |Y_{,r}|^2 + (\ell+2)(\ell-1) |Y|^2]}{\int dV r^2 \rho_H e^{\Lambda-\Phi} |Y|^2}, \quad (9)$$

where $dV = r^2 d\tilde{r} \sin \theta d\theta d\phi$ is a proper volume element, with $d\tilde{r} = e^\Lambda dr$. We will use this GR equation throughout the paper for calculating ω_μ .

One can check, that starting from Newtonian approach and switching to the simplified GR approach (2), one comes to the expression which is fully consistent with (9). According to Ref. [26], in this case one can safely replace $x_g = 2GM/(c^2 R)$ by $x_g^* = 2GM_*/(c^2 R_*)$, where M_* is the gravitational mass enclosed in a sphere of any radius R_* within the crust.

The functions (6) and (7) will be used as basic wave functions for studying magneto-elastic oscillations.

E. First-order perturbation theory

Following Refs. [48–50] we continue studying magneto-elastic oscillations using the first-order perturbation theory (FOPT) where the magnetic term \mathbf{T}_B in Eq. (3) is treated as a perturbation. We begin with the plain Newtonian approximation.

For simplicity, we study the \mathbf{B} field configurations which are axially symmetric with respect to the magnetic axis z ,

$$B_r = B_r(r, \theta), \quad B_\theta = B_\theta(r, \theta), \quad B_\phi = B_\phi(r, \theta). \quad (10)$$

The field components B_r , B_θ and B_ϕ can be arbitrary functions of r and θ satisfying magnetic flux conservation; B_r and B_θ are the poloidal field components, while B_ϕ is the toroidal one. We will also impose the mirror symmetry of $\mathbf{B}(\mathbf{r})$ -lines with respect to the magnetic equator.

Our zero-order solutions are those described in Sec. IID. Zero-order wave functions \mathbf{u} are localized in the

crust, and oscillation frequencies ω_μ are degenerate in m . A first-order correction to ω_μ will break the degeneracy owing to the Zeeman effect. The problem is similar to finding a first-order correction to a non-perturbed degenerate energy level of a quantum system (e.g., Ref. [52]). In case of not too strong Zeeman splitting, it is sufficient to use $(2\ell+1)$ zero-order wave functions \mathbf{u} corresponding to a zero-order ω_μ at given n and ℓ , and calculate then the perturbation matrix $T_{m'm}$ [of dimension $(2\ell+1) \times (2\ell+1)$] on this restricted basis of zero-order states:

$$T_{m'm} = \int_{\text{crust}} dV \mathbf{u}_{n\ell m'}^* T_B(\mathbf{u}_{n\ell m}). \quad (11)$$

This matrix naturally occurs [49], if we multiply Eq. (3) by \mathbf{u}^* and integrate over the star. Since zero-order states are confined in the crust, the integration is restricted by the crust alone. One can easily check that, for the chosen magnetic field configuration (10), the matrix $T_{m'm}$ is diagonal due to integration over ϕ from 0 to 2π . This means that the magnetic interaction does not mix the states with different m , so that labels (n, ℓ, m) retain their previous meaning (as in Sec. IID). Then any first-order ‘magnetically corrected’ oscillation frequency with fixed n and ℓ is given by the sum rule [49]:

$$\omega^2 = \omega_\mu^2 + \omega_B^2, \quad (12)$$

where

$$\omega_\mu^2 = \frac{\int dV \mathbf{u}^* \mathbf{T}_\mu}{\int dV \rho_H |\mathbf{u}^2|}, \quad \omega_B^2 = \frac{\int dV \mathbf{u}^* \mathbf{T}_B}{\int dV \rho_H |\mathbf{u}^2|}. \quad (13)$$

Hence, the true oscillation frequency ω is formally expressed via two frequencies, ω_μ and ω_B , and ω_μ can be expressed as (9).

Under the formulated assumptions the sum rule (12) is exact. It has to be true in full GR.

Since ω_μ is independent of B , all magnetic effects, including the Zeeman splitting, are incorporated in ω_B . The derivation of (12) suggests that ω_B is smaller than ω_μ , but we will extend Eq. (12) to higher B . We will present additional arguments in favor for this extension in Sec. III.

The ratios of integrals in Eqs. (13) are of similar origin. The quantity ω_B^2 can be rewritten as

$$\omega_B^2 = \frac{\int dV J_B}{\int dV \rho_H |\mathbf{u}^2|}, \quad J_B = \frac{1}{2\pi} \int_0^{2\pi} d\phi \mathbf{u}^* \mathbf{T}_B. \quad (14)$$

Here $J_B = J_B(r, \theta)$ is an effective ‘energy density’ $\mathbf{u}^* \mathbf{T}_B$ in a matter element at fixed r and θ averaged over ϕ (or, equivalently, over pulsation period if we formulated time-dependent perturbation theory). The averaging can be done analytically and separately because the dependence of $\mathbf{u}^* \mathbf{T}_B$ on ϕ in the assumed axial symmetry of \mathbf{B} is standard. This greatly simplifies the result because many $\mathbf{u}^* \mathbf{T}_B$ terms are canceled out. Taking \mathbf{T}_B from Eq. (5), the magnetic field configuration from Eq. (10), and using

the magnetic flux conservations, by direct calculation we obtain another sum rule

$$I_B \equiv 4\pi J_B = I_{Bp} + I_{Bt}, \quad (15)$$

where the terms I_{Bp} and I_{Bt} contain, respectively, only poloidal and toroidal field components.

It is convenient to write $I_{Bp} = I_{Bp0} + I_{Bp1}$. The term I_{Bp0} was obtained in [49] for describing fundamental oscillations ($n = 0$, $Y = Y_0$, see Sec. III C):

$$\begin{aligned} I_{Bp1} = & (B_\theta B_{\theta,\theta} \cot \theta + B_r B_\theta \cot \theta + r B_r B_{\theta,r} \cot \theta \\ & - B_\theta^2) P_\theta^2 |Y|^2 - (B_\theta B_{\theta,\theta} + B_r B_\theta + r B_r B_{\theta,r}) P_\theta P_{,\theta\theta} \\ & \times |Y|^2 - B_\theta^2 P_{,\theta} P_{,\theta\theta\theta} |Y|^2 + [B_\theta^2 P_\theta^2 - (B_\theta B_{\theta,\theta} \\ & + B_\theta^2 \cot \theta + 2B_r B_{r,\theta} + B_r B_\theta + r B_r B_{\theta,r}) P P_\theta \\ & + B_r (B_{\theta,\theta} + B_\theta \cot \theta + r B_{\theta,r\theta} + r B_{\theta,r} \cot \theta \\ & - B_{r,\theta\theta} + B_{r,\theta} \cot \theta) P^2] |Y|^2 (m/\sin \theta)^2. \end{aligned} \quad (16)$$

Indices θ and r after commas in the subscripts again denote respective partial derivatives; $P = P_\ell^m(\cos \theta)$.

The second term I_{Bp1} reads

$$\begin{aligned} I_{Bp1} = & r Y^* P_{,\theta} B_r [Y_{,r} P_{,\theta} (B_\theta \cot \theta - 2B_r - r B_{r,r}) \\ & - Y_{,r} B_\theta P_{,\theta\theta} - r Y_{,rr} B_r P_{,\theta}] - r Y^* Y_{,r} B_\theta P_{,\theta} \\ & \times [P_{,\theta} B_r \cot \theta + P_{,\theta} B_{r,\theta} + P_{,\theta\theta} B_r \\ & - (m/\sin \theta)^2 P B_r] - r Y^* P B_r (m/\sin \theta)^2 \\ & \times [P_{,\theta} B_\theta Y_{,r} - P (B_{\theta,\theta} + B_\theta \cot \theta - 2B_r) Y_{,r} \\ & + r P B_r Y_{,rr} + r P B_{r,r} Y_{,r}]. \end{aligned} \quad (17)$$

It is needed for studying oscillations with radial nodes ($n > 0$).

Finally, in the presence of toroidal field we obtain

$$\begin{aligned} I_{Bt} = & |Y|^2 P B_\phi (m/\sin \theta)^2 [(m/\sin \theta)^2 P B_\phi \\ & - P_{,\theta\theta} B_\phi - 2P_{,\theta} B_{\phi,\theta} + P_{,\theta} B_\phi \cot \theta \\ & + P B_{\phi,\theta} \cot \theta - P B_{\phi,\theta\theta} - P B_\phi / (\sin \theta)^2]. \end{aligned} \quad (18)$$

Equations (16)–(18) make the integration over dV in the nominator of (14) quite feasible. It is reduced to the integrations over θ (from 0 to π) and r (from R_1 to R_2). The integration in the denominator is also simplified, as detailed in [49].

Now we return from the Newtonian approach to the simplified GR approach (Sec. IIB). As a result, Eq. (14) takes the same form as in [49]:

$$\begin{aligned} \omega_B^2 = & \frac{(1-x_g) \int_{R_1}^{R_2} dr r^2 \int_0^\pi \sin \theta d\theta I_B}{4\pi \int_{R_1}^{R_2} dr r^2 \rho_H \int_0^\pi \sin \theta d\theta |\mathbf{u}^2|} \\ = & \frac{(1-x_g) \int_{\text{crust}} dV I_B}{4\pi \Xi(\ell, m) \int_{\text{crust}} dV |Y|^2 \rho_H r^2}, \end{aligned} \quad (19)$$

where dV is the same as in Eq. (9) (including angular integration, with constant Λ), and the normalization coefficient $\Xi(\ell, m)$ reads [49]

$$\Xi(\ell, m) = \frac{2\ell(\ell+1)(\ell+m)!}{(2\ell+1)(\ell-m)!}. \quad (20)$$

The factor $(1 - x_g)$ accounts for gravitational redshift of the squared oscillation frequency, and r is circumferential radius. The field $\mathbf{B}(r)$ is treated as the magnetic field in the crustal reference frame. While calculating I_B from Eqs. (16)–(18), it is desirable to calculate radial derivatives as prescribed in Sec. IIB. This was not done in our previous work (Refs. [49, 50]). This is not an error, but rather a trick to be more consistent with GR.

Note that the function $Y(r)$ was not included in I_B and in the denominator of the expression for ω_B^2 in Ref. [49]. That paper was devoted to fundamental oscillations in which case $Y(r)$ was set constant (see Sec. IIIC) and naturally dropped in the ratio of integrals.

So far we have not used the assumed symmetry of \mathbf{B} -field lines with respect to the magnetic equator. Imposing this assumption, we evidently obtain that oscillation frequencies with $m \neq 0$ and opposite m become equal. Accordingly, the frequencies can be labeled by the index m which runs the integer values $m = 0, 1, \dots, \ell$. The frequencies with $m = 0$ are non-degenerate, while those with $m > 0$ are now degenerate twice.

F. Alfvén wave problem

Calculations in Sec. IIE have been performed using the FOPT with respect to the magnetic field strength. It is expected to be accurate for describing the Zeeman splitting at not too high magnetic fields. Its firm applicability conditions deserves further attention, particularly, in view of the Alfvén wave problem.

The theory assumes vanishing elastic shear stresses at the boundaries of crystallized matter. Nevertheless, in the presence of Alfvén perturbations, there are additional magnetic stresses, which should appear in higher-order versions of the perturbation theory. Alfvén perturbations can spread magneto-elastic oscillations outside the crust. This important effect has been studied in many publications, e.g., [27, 28, 30, 33–38]. These studies have been mainly restricted to axially symmetric perturbations which drive the oscillations only with $m = 0$ (see Sec. III). More work is required to explore all consequences of this effect.

III. TOROIDAL MAGNETIC FIELDS

A. Squared magnetic frequency ω_B^2

Here we focus on the case of pure toroidal magnetic field \mathbf{B} determined by $B_\phi(r, \theta)$ in Eq. (10). This case has attracted little attention, but it is important and very simple. To avoid discussing the Alfvén wave problem (Sec. IIF), we restrict ourselves to the field configurations confined fully in the solid crust. The magneto-elastic oscillations cannot then spread outside. Such toroidal fields should be supported by poloidal electric currents

located in the crust. In this case in Eq. (19) we have $I_B = I_{Bt}$.

By way of illustration, we consider a toroidal magnetic field of the form

$$B_\phi = B_0 \sin \theta \psi(x), \quad x = \frac{R_2 - r}{R_2 - R_1}. \quad (21)$$

Here B_0 is the maximum field in the crust. The dependence of B_ϕ on r is now determined by a dimensionless function $\psi(x)$ of a dimensionless depth x that varies from $x = 0$ at the outer surface of the crystalline matter ($r = R_2$) to $x = 1$ at the crust bottom ($r = R_1$). The function $r\psi(x)$ is often called the source function (e.g. [53]). We assume that $\psi \rightarrow 0$ as $x \rightarrow 0$ and $x \rightarrow 1$ to avoid electric currents at both boundary surfaces. The maximum value $\psi = 1$ occurs at the depth, where B_ϕ reaches its maximum. Note that in our calculations R_2 has been taken only slightly lower than R , so that the difference can be safely neglected in final expressions.

The dependence of B_ϕ on θ in Eq. (21) is fixed. Then $B_{\phi,\theta} = B_\phi \cot \theta$ and $B_{\phi,\theta\theta} = -B_\phi$, and Eq. (18) reduces to

$$I_{Bt} = |Y|^2 \ell(\ell + 1) \frac{m^2 P^2 B_\phi^2}{\sin^2 \theta}, \quad (22)$$

where the differential equation for $P = P_\ell^m(\cos \theta)$ has been used (e.g., [51]). Now the integration over θ in the nominator of (19) is carried out analytically, and we come to the very simple expression

$$\omega_B^2 = (1 - x_g) \frac{m^2 B_0^2 \int_{R_1}^{R_2} dr \psi^2 |Y|^2 r^2}{4\pi \int_{R_1}^{R_2} dr \rho_H |Y|^2 r^4}. \quad (23)$$

It shows the Zeeman splitting of oscillation frequencies ω , in which $\omega_B^2 \propto m^2$ and the Legendre polynomials $P_\ell^m(\cos \theta)$ are integrated out. At $m = 0$ we have $\omega_B = 0$, and the total oscillation frequency in Eq. (12) becomes $\omega = \omega_\mu$, being independent of B . In Eq. (23) we are left with the ratio of two simple radial integrals which can be easily computed for any given model of the neutron star crust and any meaningful function $\psi(r)$.

B. Neutron star models

For illustration, we use neutron star models based on one equation of state (EOS) of dense matter called the BSk21 EOS. It belongs to a family of well elaborated Brussel-Montreal EOSs. They are unified: energy-density functionals, employed for constructing the EOSs in the crust and the core, are the same. The core is assumed to contain nucleons, electrons and muons. The BSk21 crust consists of electrons and spherical atomic nuclei. In deep crustal layers ($\rho \geq 4.28 \times 10^{11} \text{ g cm}^{-3}$) there appear free neutrons, and near the crust-core interface ($\rho_{cc} \approx 1.34 \times 10^{14} \text{ g cm}^{-3}$) there occurs an admixture of free protons.

Various properties of neutron stars with the BSk21 EOS are described by convenient analytic approximations in Ref. [54]. The maximum mass of the neutron star mass is $2.27 M_\odot$; its radius $R = 11.25$ km. The neutron star with the canonical mass of $1.4 M_\odot$ has radius $R = 12.60$ km, and the core radius $R_1 = 11.55$ km. A lighter $1 M_\odot$ star has $R = 12.48$ km and $R_1 = 10.92$ km. A very massive $2.2 M_\odot$ star has $R = 11.81$ km and $R_1 = 11.39$ km. We will begin with the $1.4 M_\odot$ model and then extend the results over the $(1 - 2.2) M_\odot$ mass range.

We will use the same microphysics of the crust as in Refs. [26, 49, 50].

C. Fundamental modes ($n = 0$): Theory

Here, using FOPT, we study fundamental oscillation modes, with nodeless ($n = 0$) radial wave function $Y(r)$. This case is important because it corresponds to magnetar QPOs with frequencies lower than a few hundred Hz. Corresponding wave functions are known (e.g. Ref. [25]) to be nearly independent of r , and can be approximated by a constant, $Y \rightarrow Y_0$. This constant drops out in the ratios of integrals in all the expressions for ω_μ and ω_B , e.g., in Eqs. (9) and (23).

Then the exact GR equation (9) becomes

$$\omega_\mu^2 = \frac{1}{4}(\ell + 2)(\ell - 1)\omega_{\mu 0}^2, \quad (24)$$

where $\omega_{\mu 0}$ is the frequency of the lowest torsion fundamental mode ($\ell = 2$),

$$\omega_{\mu 0}^2 = \frac{4 \int_{\text{crust}} dV \mu}{\int_{\text{crust}} dV r^2 \rho_H e^{\Lambda - \Phi}} = (1 - x_g) \frac{8W_\mu}{3I_0}. \quad (25)$$

The last expression is obtained by employing our simplified GR model of the crust (Sec. II B), in which $e^{\Phi - \Lambda} \rightarrow (1 - x_g)$. Accordingly, $\omega_{\mu 0}^2$ is determined by I_0 , which is the standard moment of inertia of the crust in the crustal reference frame, and by W_μ , which is the shear modulus μ integrated over the crust in the same frame. In calculations, we use the well known expression $\mu = 0.1194 n_i Z^2 e^2 / a_i$ [55], where n_i is the number density of atomic nuclei, Ze is the electric charge of one nucleus, and $a_i = (4\pi n_i / 3)^{-1/3}$ is the ion-sphere radius. Since the Coulomb binding energy per one nucleus is $\approx 0.9 Z^2 e^2 / a_i$, we have $W_\mu = 0.133 W_C$, W_C being the Coulomb energy of the crust.

As for the squared magnetic frequency ω_B , given by (23), it can be written as

$$\omega_B^2 = m^2 \omega_{B 0}^2, \quad \omega_{B 0}^2 = (1 - x_g) \frac{2W_B}{I_0} \quad (26)$$

where

$$W_B = \int_{\text{crust}} dV \frac{B_\phi^2}{8\pi} = \frac{\kappa}{3} B_0^2 R_2^2 (R_2 - R_1), \quad (27)$$

is the magnetic energy of the crust and

$$\kappa = \int_0^1 (r/R_2)^2 \psi^2(x) dx, \quad (28)$$

is a dimensionless numerical coefficient. This coefficient depends mostly on $\psi(x)$. Also, it slightly depends on a stellar model because of the factor $(r/R_2)^2$ which slowly decreases from its maximum value 1 at $x = 0$ to $(R_1/R_2)^2$ at the crust bottom. For B_ϕ configurations different from (21) a numerical factor in (26) will differ from 2.

According to Eqs. (25) and (26), physical meanings of $\omega_{\mu 0}$ and $\omega_{B 0}$, are similar: while the former is determined by the Coulomb energy of the crust, the latter is determined by the magnetic energy.

To be specific, we will mainly use

$$\psi_0(x) = 16x^2(1 - x)^2, \quad (29)$$

although we will try other $\psi(x)$ which renormalize κ . Neglecting the factor $(r/R_2)^2 \approx 1$ in (28), we obtain an estimate $\kappa_0 \approx 128/315 = 0.40635$.

Now we can rewrite Eq. (26) as

$$\omega_B^2 = m^2 \omega_{B 0*}^2 B_*^2, \quad B_* = \frac{B_0}{10^{15} \text{ G}}, \quad (30)$$

where $\omega_{B 0*}$ is a convenient measure of ω_B at a typical value of $B_0 = 10^{15}$ G; $\omega_{B 0*}$ is independent of ℓ , m as well of a specific value of B_0 , but depends on $\psi(x)$.

Then the frequency of any fundamental magneto-elastic oscillation mode ($n = 0$, any allowable ℓ and m), as calculated in FOPT, is determined by the two auxiliary frequencies, $\omega_{\mu 0}$ and $\omega_{B 0*}$, one and the same for a given stellar model. Note that $\omega_{B 0} \propto B_0 \sqrt{\kappa}$.

In cyclic frequencies $\nu = \omega / (2\pi)$ we have

$$\nu_{\ell m}^2 = \frac{1}{4}(\ell + 2)(\ell - 1)\nu_{\mu 0}^2 + m^2 \nu_{B 0*}^2 B_*^2, \quad (31)$$

with the two constants, $\nu_{\mu 0}$ and $\nu_{B 0*}$.

As discussed in Refs. [25, 26], the simplistic ℓ -dependence of (25) and (31) can be violated at $\ell \gg 10$. Equation (31) can also become inaccurate at large m but this is not vitally important for applications (see Sec. IV).

D. Fundamental modes for a $1.4 M_\odot$ star

Here we discuss fundamental magneto-elastic oscillation frequencies calculated for a $1.4 M_\odot$ neutron star model with the BSK21 EOS.

We begin with the FOPT results assuming $\psi(x) = \psi_0(x)$, see Eq. (29). The frequencies are given by Eq. (31), being determined by the two numbers, $\nu_{\mu 0}$ and $\nu_{B 0*}$, listed in Table I.

Figure 1 presents the frequencies $\nu_{\ell m}$ for $\ell = 2, \dots, 10$ and all allowable m at $\nu \leq 130$ Hz as a function of B_0 . One can see nine bunches of $\nu(B_0)$ curves. Each bunch corresponds to a fixed ℓ and contains $\ell + 1$ curves (with m from 0 to ℓ) plotted in one color. The lowest (dashed)

TABLE I. Eight auxiliary constant frequencies (in Hz), which determine magneto-elastic oscillation spectrum (different ℓ and m) of fundamental modes ($n = 0$, first two values), and ordinary modes (Sec. III F) with $n = 1$ (next three values) and $n = 2$ (last three values) for a $1.4 M_\odot$ neutron star with the BSk21 EOS.

| $\nu_{\mu 20}$ | ν_{B0*} | $\nu_{\mu 1}$ | $\delta\nu_{\mu 1}$ | $\delta\nu_{B1*}$ | $\nu_{\mu 2}$ | $\delta\nu_{\mu 2}$ | ν_{B2*} |
|----------------|-------------|---------------|---------------------|-------------------|---------------|---------------------|-------------|
| 23.06 | 4.192 | 829.7 | 12.98 | 15.98 | 1327 | 14.87 | 22.96 |

curve in a bunch refers to $m = 0$. In our approximation, it is independent of B_0 , being solely determined by the elastic shear, $\nu = \nu_\mu$. With increasing m , other (solid) curves in a bunch grow up, demonstrating Zeeman splitting. Neglecting the Zeeman effect leads to the loss of all oscillation modes with $m > 0$.

As long as $B_0 \ll 10^{14}$ G, the spitting is almost invisible, but it becomes more pronounced with increasing B_0 . Note that some low- m modes are nearly indistinguishable in Fig. 1. For instance, the frequencies with $\ell = 2$ at $m = 0$ and $m = 1$ nearly coincide (although they would diverge at $B_0 \gtrsim 5 \times 10^{15}$ G). With increasing ℓ , the number of Zeeman components in a bunch grows up and the Zeeman splitting becomes visible at lower B_0 .

It is important to mention crossings of pairs of modes from different bunches at sufficiently high B_0 . Such crossings turn usually to well known quasi-crossings due to resonance interactions of the modes (see, e.g. Ref. [52]). These effects are not described by our FOPT approach: one needs to include higher-order perturbation terms. This can be an interesting problem for the future.

Figure 2 is a sketch of the same picture, as in Fig. 1, but extended to higher frequencies by including additional bunches with ℓ from 11 to 14. To avoid plotting over-dense Zeeman splittings at high ℓ , each bunch is specified by the frequencies of the lowest ($m = 0$) and highest ($m = \ell$) modes drawn in one color. A space between these limiting frequencies is darkened. Roughly speaking, in the $\nu - B_0$ plane one can distinguish domains of two types: forbidden (white) and allowed (darkened) ones. The region of rather low ν and B_0 , where neighboring bunches do not cross, contains a lot of white domains which are forbidden for oscillations of a given star. The darkened domains at higher ν and B_0 are densely filled with Zeeman structures. If observed oscillation frequencies fall into these domains, it would be easy to explain them for the given star. One needs $B_0 \gtrsim 10^{15}$ G for reaching these ‘allowable’ domains at $\nu \gtrsim 140$ Hz, but $B_0 \gtrsim 3 \times 10^{15}$ G at $\nu \lesssim 140$ Hz.

So far we have studied only one radial profile (29) of $B_\phi(r)$ through the neutron star crust. In Fig. 3 we plot this profile by the thick black line (line 0). This profile is centered at $x = 1/2$, just in the middle between the inner and outer boundaries, R_1 and R_2 . For exploring the sensitivity of our results to the profile shape, we have considered three more $\psi(x)$ models plotted in Fig. 3 by thinner lines 1, 2, and 3. The profiles 1 and 2 are

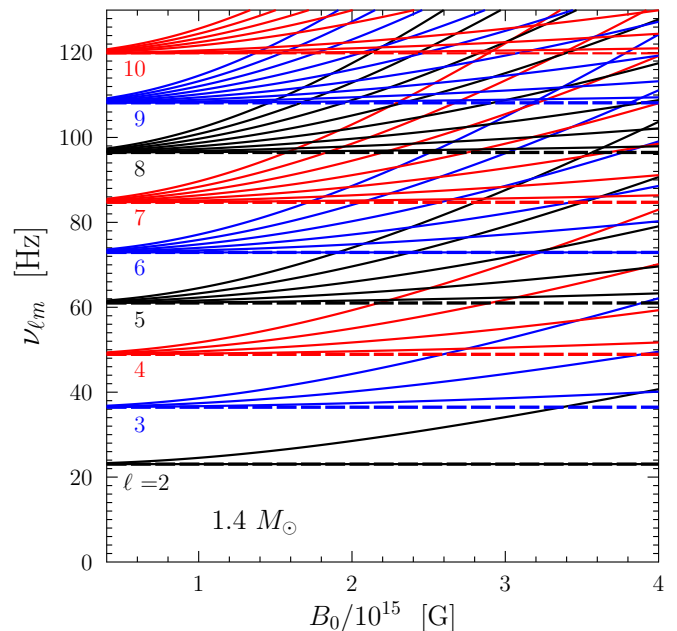


FIG. 1. Frequencies of fundamental ($n = 0$) magneto-elastic oscillations, as calculated using FOPT, versus maximum toroidal magnetic field B_0 in the crust for a $1.4 M_\odot$ neutron star model (BSk21 EOS). Shown are the bunches of modes with ℓ from 2 to 10, and m from 0 to ℓ in each branch. The frequencies with $m = 0$ (dashed lines) are independent of B .

slightly narrower; the peak of profile 1 is shifted to the surface, while the peak of profile 2 is shifted to the stellar core. The shifts are symmetric with respect to $x = 1/2$. The profile 4 is again centered at $x = 1/2$ being noticeably narrower than other profiles. Actually, we just set $\psi_4(x) = \psi_0^2(x)$.

Corresponding oscillation frequencies are compared in Fig. 4. For clarity, we plot only two oscillation bunches, for $\ell = 4$ and 7.

The thick black lines refer to our basic model; they are the same as in Fig. 1. Other lines in Fig. 4 refer to models 1, 2, and 3. Changing $\psi(x)$ renormalizes the frequency ν_{B0*} in Eq. (31). Instead of $\nu_{B0*} = 4.19$ Hz for model 0 in Table I, we would have 3.87 Hz, 3.81 Hz and 3.59 Hz, for models 1, 2 and 3, respectively. The renormalized ν_{B0*} for models 1 and 2, as well as respective oscillation spectra in Fig. 4, appear to be very close. The frequencies for model 1 are slightly higher because of somewhat higher crustal magnetic energy W_B [see Eq. (27)] due to the factor $(r/R_2)^2$ under the integral in (28). The lower W_B , the weaker magnetic field effect on oscillation frequencies.

Note a funny effect of frequency degeneracy in Fig. 4: accidentally, the oscillation frequency at $\ell = 7$ and $m = 6$ for the basic model 0 coincides with the frequency at $\ell = 7$ and $m = 7$ for model 4, and the two curves merge. Similar degeneracies are discussed below in Sec.

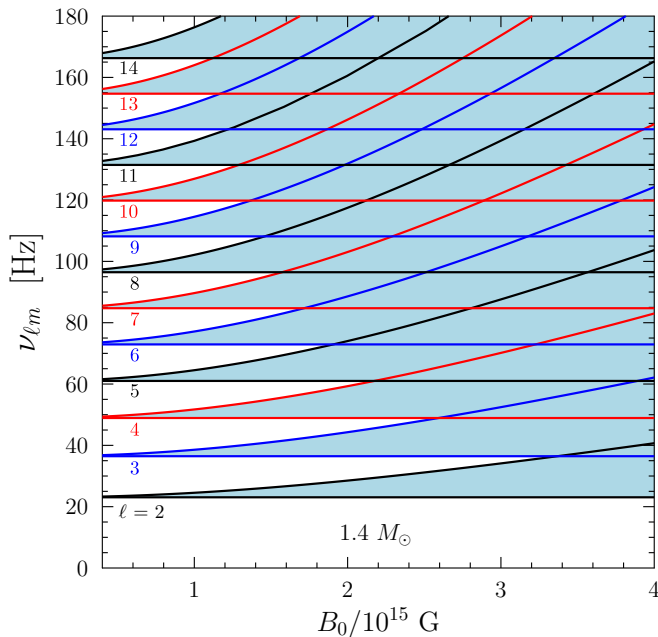


FIG. 2. Same as in Fig. 1 in a sketchy manner but for higher number of bunches ($\ell \leq 14$). Frequencies in each bunch fall in darkened space between lowest ($m = 0$) and highest ($m = \ell$) frequencies. See the text for details.

IV.

E. Restricted variational estimates

So far we have presented only FOPT calculations of magneto-elastic oscillation frequencies. Here we check these results using restricted variational estimates. To this aim, we use the expression $\nu^2\{Y\} = \nu_\kappa^2\{Y\} + \nu_B^2\{Y\}$ as a functional of the radial wave function $Y(r)$. In the FOPT, this wave function is constant, $Y = Y_0$, and drops out of the theory. Using $Y(r)$ as a variational function for minimizing $\nu^2\{Y\}$ allows us to estimate the validity of FOPT and possible deviations of ν from the FOPT values.

For studying the fundamental oscillations, the variational function $Y(r)$ should have no nodes at $R_1 \leq r \leq R_2$. Also, it should satisfy proper boundary conditions ($Y_{,r}(r) = 0$ at $r = R_1$ and R_2). The functionals $\nu_\kappa^2\{Y\}$ and $\nu_B^2\{Y\}$ are given by Eqs. (9) and (23), respectively. As before, we employ our $1.4 M_\odot$ stellar model. The radial dependence of B_ϕ is given by Eq. (29). The variational function has been chosen in the form

$$Y(r) = [1 + w \sin^2(\pi x/2)] Y_0, \quad (32)$$

where x is the same dimensionless depth as in Eq. (21), and w is a single variational parameter. Then $Y(r)$ varies monotonically from Y_0 at $r = R_2$ to $(1 + w)Y_0$ at $r = R_1$. We have tried some other functions which amplified

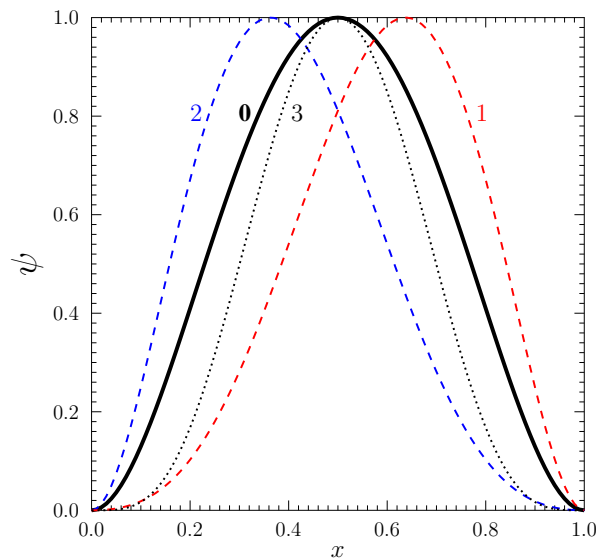


FIG. 3. Four versions of the function $\psi(x)$, that determines the radial behavior of B_ϕ , versus dimensionless depth x within the crystalline layer. The thick line 0 is the basic version, Eq. (29). Other versions 1–3 are for checking sensitivity of oscillation frequencies to the shape of $B_\phi(r)$ profile.

variations near the surface or near the crust bottom, but they have not led to much better variational estimates of ν . Since our approach is oversimplified anyway (e.g., it neglects possible mixtures of states with different ℓ and m), we would not like to complicate the variational function.

Figure 5 compares the FOPT frequencies, calculated at $\ell = 4$ and $\ell = 7$ (black curves) with corresponding variational estimates (blue curves) for $B_0 \leq 4 \times 10^{15}$ G. Variational estimates are naturally smaller than the FOPT values. As expected, the difference grows up with increasing B_0 and m . At $\ell = 7$ the difference is more pronounced, than at $\ell = 4$, and becomes visible at lower B_0 . Otherwise, both approaches seem to be in a reasonable qualitative agreement. This allows us to expect that using FOPT at $B_0 \lesssim 4 \times 10^{15}$ G does not lead to serious errors.

F. Zeeman splitting of fine structures of ordinary modes ($n > 0$)

Let us focus on ordinary magneto-elastic modes which exist in addition to fundamental modes and which are characterized by the presence of nodes of the radial wave function $Y(r)$. Typical frequencies of these modes are higher than several hundred Hz. We restrict ourselves by the FOPT approximation.

The ordinary modes are different from fundamental ones. In the absence of a magnetic field, for a fixed $n > 0$ there exist a family of closely spaced frequencies $\nu_{\mu n \ell}$

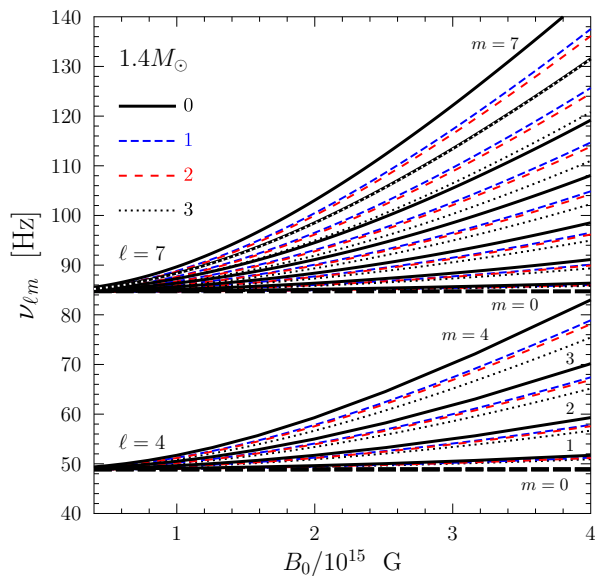


FIG. 4. Sensitivity of magneto-elastic oscillation frequencies to the radial dependence of B_ϕ . We show two bunches of oscillation modes, with $\ell=4$ and 7 , versus B_0 for four versions of the function ψ in Fig. 3. See the text for details.

which slowly grow up with increasing $\ell = 2, 3, \dots$. Their spectrum resembles fine structure of atomic energy levels. Such spectra have been studied in Ref. [26] in full GR, with the result that for any fixed n they are accurately fitted as

$$\nu_{\mu n \ell}^2 = \nu_{\mu n}^2 + (\ell + 2)(\ell - 1)\delta\nu_{\mu n}^2, \quad (33)$$

with only two constant auxiliary frequencies, $\nu_{\mu n}$ and $\delta\nu_{\mu n}$.

The magnetic correction $\nu_{Bn\ell m}$ can be calculated using Eq. (23) with the wave functions $Y_{n\ell}(r)$ computed in the same way as described in Ref. [49]. The result can be written in the form similar to Eq. (30),

$$\nu_{Bn\ell m}^2 = m^2\nu_{Bn*}^2 B_*^2, \quad (34)$$

where ν_{Bn*} is a single ‘magnetic’ auxiliary frequency for a fixed n . It is independent of ℓ because $Y_{n\ell}(r)$ is nearly independent of ℓ at $n > 0$ [26].

Now a squared total FOPT frequency of an ordinary magneto-elastic oscillation is

$$\nu_{nlm}^2 = \nu_{\mu n}^2 + (\ell + 2)(\ell - 1)\delta\nu_{\mu n}^2 + m^2\nu_{Bn*}^2 B_*^2. \quad (35)$$

It is determined by the three constants, $\nu_{\mu n}$, $\delta\nu_{\mu n}$ and ν_{Bn*}^2 for a given fine structure with fixed n .

For our $1.4 M_\odot$ star, these constants, with $n = 1$ and 2 , are listed in Table I: $\nu_{\mu n}$ and $\delta\nu_{\mu n}$ are taken from [26], while the constants ν_{Bn*} are original, calculated assuming $\psi(x) = \psi_0(x)$.

For example, Figs. 6 and 7 show the fine structure and its Zeeman splitting for a family of oscillation frequencies

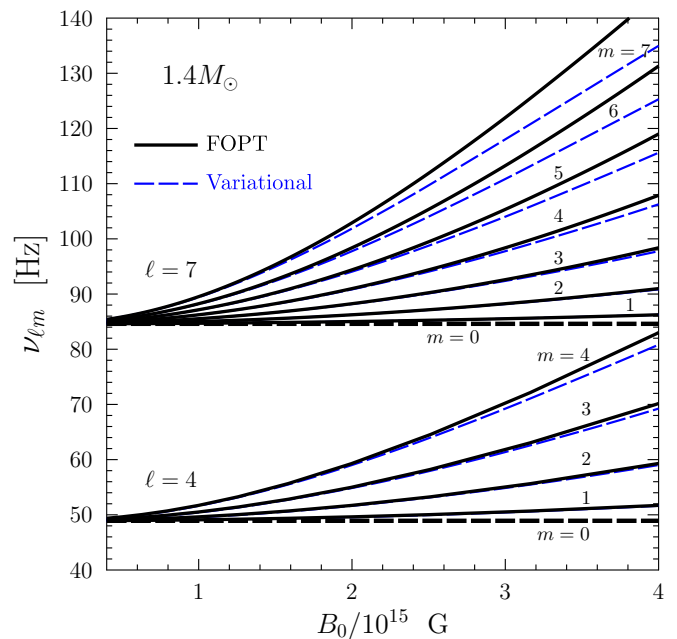


FIG. 5. Comparing oscillations frequencies calculated using FOPT with variational estimates. Shown are magneto-elastic oscillation frequencies versus B_0 for two bunches of modes with $\ell=4$ and 7 at various m .

with $n = 1$, for values of ℓ from 2 to 6 , and all values of m . Bunches of curves with higher $\ell = 7, 8, \dots$ are not plotted for simplicity. Figure 6 is restricted by $B_0 \leq 10^{15}$ G and by a narrow frequency interval of the width ≈ 10 Hz. Figure 7 is an extension to $B_0 \leq 4 \times 10^{15}$ and to higher ν for demonstrating a general view.

The fine structure itself ($B_0 = 0$) is shown by horizontal dashed lines. The lowest frequency is 830.1 Hz. All five plotted frequencies fall within the 4 Hz window.

The Zeeman effect splits the fine-structure components into the bunches of modes with the same ℓ but different m . Because the difference of frequencies between fine-structure components is small, the bunches start to cross (Fig. 6) at smaller $B_0 \lesssim 10^{15}$ G than for the fundamental modes (Sec. III D).

At $B_0 \gtrsim 10^{15}$ G one gets distinctly different bunches (Fig. 7). These can be numbered by the index m , and the curves within any bunch can be numbered by ℓ . Such rearrangement of the structure of bunches resembles the well known Paschen-Back effect in atomic physics (e.g., [52]). The higher ℓ , the lower B_0 at which the rearrangement occurs.

Adding oscillation frequencies with higher ℓ , we would obtain a dense sequence of magneto-elastic oscillations at the same $n = 1$. Any high-frequency magnetar QPO observed in this range would be consistent with this theory. This adds to our discussion (Sec. III D) of allowed (darkened) regions of oscillation frequencies in Fig. 2.

The situation with cases of two and more nodes ($n \geq 2$)

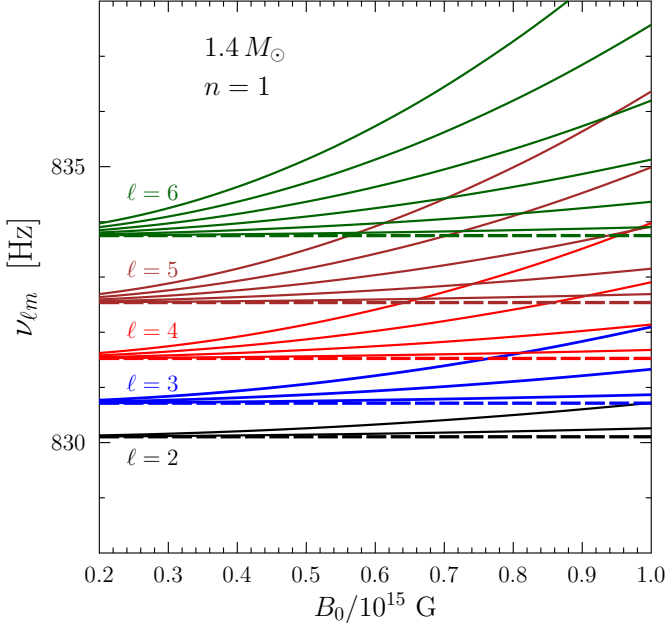


FIG. 6. Zeeman splitting versus B_0 of fine structure components of oscillations with one radial node. We plot the splitting for bunches with ℓ from 2 to 6. Adding bunches with larger ℓ would fill the range of higher ν . For example, at $\ell=7, 8, 9$ and 10 , the basic fine-structure frequencies (33) $\nu_{\mu 1\ell}$ are 835.2, 836.8, 8.38.6 and 840.6, respectively.

is similar. The frequencies of these oscillations are even higher. For instance, the lowest frequency for the same neutron star model at $n = 2$ is 1.327 kHz.

G. Self-similarity. Different masses

Table I contains eight constants which are sufficient to calculate frequencies of magneto-elastic oscillations with $n = 0, 1$ and 2 , for our $1.4M_\odot$ neutron star model with the toroidal magnetic field geometry defined by Eq. (29).

Now we employ the self-similarity relations [26], which allow one to extend these results to a range of stellar masses with fixed EOS. For instance, in Ref. [26], the auxiliary frequencies denoted here as $\nu_{\mu 0}$, as well as $\nu_{\mu n}$ and $\delta\nu_{\mu n}$ with $n > 0$, were calculated at $M/M_\odot = 1, 1.2, 1.4, \dots, 2.2$ (the BSk21 EOS) and fitted by simple expressions. To simplify using these results, all frequencies were fitted [26] by analytic functions of neutron star mass and radius,

$$\delta\nu_{\mu n} = \frac{\sqrt{1-x_g} \delta f_{\mu n}}{R_{10} \sqrt{1 + \delta\alpha_{\mu n} x_g + \delta\beta_{\mu n} x_g^2}}, \quad (36)$$

$$\nu_{\mu n} = \frac{M_1}{R_{10}^2} f_{\mu n} \sqrt{1 + \alpha_{\mu n} x_g + \beta_{\mu n} x_g^2}, \quad (37)$$

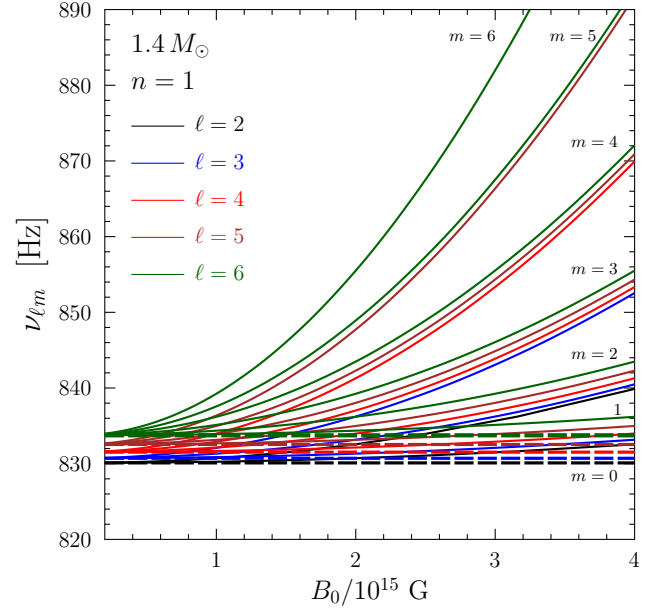


FIG. 7. Same as in Fig. 6 but for a wider range of B_0 and ν .

where x_g is defined in Eq. (2); $R_{10} = R/10$ km, $M_1 = M/M_\odot$; $f_{\mu n}$, $\alpha_{\mu n}$, $\beta_{\mu n}$, $\delta f_{\mu n}$, $\delta\alpha_{\mu n}$ and $\delta\beta_{\mu n}$ are fit parameters. For $n=0, 1$ and 2 we reproduce these fit parameters in Table II. Note that $\nu_{\mu 0}$, $\delta\nu_{\mu 1}$ and $\delta\nu_{\mu 2}$ have to be calculated using Eq. (36), while $\nu_{\mu 1}$ and $\nu_{\mu 2}$ – using Eq. (37).

Here we compute the magnetic auxiliary frequencies $\nu_{n B_*}$ at $n=0, 1$ and 2 on the same grid of masses. Considering self-similarity of such frequencies in the same manner as in [26], we obtain that they can be fitted by

$$\delta\nu_{B n^*} = \frac{\sqrt{1-x_g} \delta f_{B n}}{R_{10} \sqrt{1 + \delta\alpha_{B n} x_g + \delta\beta_{B n} x_g^2}}, \quad (38)$$

where $\delta f_{B n}$, $\delta\alpha_{B n}$ and $\delta\beta_{B n}$ are the fit parameters which we list in Table II.

As a result, Table II contains 24 fit parameters which allows one to calculate all FOPT frequencies of magneto-elastic oscillations for fundamental modes ($n = 0$), and two series of ordinary modes ($n = 1$ and 2) in neutron stars with the BSk21 EOS at any mass M ranged from $1 M_\odot$ to $2.2 M_\odot$. These stars possess toroidal magnetic field localized in their crust and obeying Eq. (29).

Note that in the indicated mass range the radii R (in km) of these stars can be fitted by

$$R = R_{\min} + 3.552 (M/M_{\max}) \sqrt{1 - (M/M_{\max})}, \quad (39)$$

where $R_{\min} = 11.246$ km is the radius of the star with the maximum mass $M_{\max} = 2.27 M_\odot$. The maximum relative fit error is 0.6 percent. This facilitates calculations of oscillation frequencies.

TABLE II. Fit parameters in Eqs. (36), (37) and (38) which determine magneto-elastic oscillations of fundamental modes ($n = 0$) and ordinary modes with $n = 1$ and $n = 2$ for neutron stars models with the BSk21 EOS at $M \geq 1 M_\odot$

| n | $\delta f_{\mu n}$ [Hz] | $\delta \alpha_{\mu n}$ | $\delta \beta_{\mu n}$ | $f_{\mu n}$ [Hz] | $\alpha_{\mu n}$ | $\beta_{\mu n}$ | δf_{Bn^*} [Hz] | $\delta \alpha_{Bn^*}$ | $\delta \beta_{Bn^*}$ |
|-----|-------------------------|-------------------------|------------------------|------------------|------------------|-----------------|------------------------|------------------------|-----------------------|
| 0 | 44.59 | 2.411 | -1.968 | 0 | - | - | 9.940 | 5.662 | -4.504 |
| 1 | 24.61 | 2.166 | -1.801 | 1171.7 | -1.508 | 1.326 | 40.00 | 6.779 | -5.381 |
| 2 | 27.35 | 1.750 | -1.340 | 1821.5 | -1.342 | 1.163 | 61.01 | 8.000 | -5.923 |

The suggested analytic fits are fairly accurate: the fitted oscillation frequencies do not deviate from the initially calculated ones by more than a few percent. This is much better than needed for analyzing current data on magnetar QPOs (Sec. IV). Besides, one cannot seriously believe that magnetars possess purely toroidal magnetic fields of this specific geometry, and that the FOPT is the best tool to describe the oscillations.

Moreover, we had no intention to obtain so accurate fits: they seem to result from natural self-similarity relations [26]. As shown in [26], similar relations are valid for a wide class of EOSs. We do not consider other EOSs here because we do not expect to obtain anything qualitatively different.

One can formulate other self-similarity relations which will be discussed in the next section.

IV. DISCUSSION

We have calculated frequencies of magneto-elastic oscillations in the crust of neutron stars with toroidal magnetic fields of specific geometry, (21) and (29), fully localized in the crust. This allows us to avoid studying leakage of Alfvén perturbations outside the crust (Sec. II F) and makes the theory more reliable. The assumed $\mathbf{B}(\mathbf{r})$ structure is just a convenient simplified toy model, which can reflect general features of magneto-elastic oscillations.

The QPO data were mostly obtained from observations of the giant flare from the SGR 1900+14 and the hyperflare from the SGR 1806-20. The QPO frequencies were found by processing and reprocessing the observed lightcurves of these flaring magnetars, e.g., Refs. [5, 7-10]. The results are summarized, for instance, in Ref. [46]. The QPOs at frequencies 28, 53, 84 and 155 Hz were detected from the giant flare of SGR 1900+14. The QPOs at 18, 26, 30, 92 and 150 Hz (as well as at 17, 21, 36, 59 and 116 Hz with a lower significance) were found from the hyperflare of SGR 1806-20.

Nevertheless, there was one publication, Ref. [11], based on a procedure of removing noise of observed signals at $\nu \lesssim 150$ Hz using some original version of Bayesian analysis. It did not confirm statistical significance of all low-frequency QPOs reported previously from both flares but discovered two new QPOs at 9.2 and 7.7 Hz from the SGR 1806-20 hyperflare. An additional confirmation of these results, reported by one

group in one publication, would be welcome but it has not appeared in six years. In its absence, we follow Refs. [23, 46] and employ the familiar set of observable QPOs which was accepted and analyzed in many publications.

Although strict explanation of the data with our toy model cannot be serious, Figs. 8 and 9 present two illustrative possibilities.

In Fig. 8 we compare the frequencies of three QPOs (dotted lines), supposed to be observed from the giant flare of SGR 1900+14, with the frequencies of magneto-elastic oscillations calculated (Fig. 1) for our $1.4 M_\odot$ magnetar model at different values of B_0 . By choosing $B_0 = (1.7 - 1.9) \times 10^{15}$ G, we can explain these QPOs assuming excitation of oscillations with certain ℓ and m . The QPO at 28 Hz corresponds to $\ell = 2$ and $m = 2$; the QPO at 53 Hz - to $\ell = 4$ and $m = 3$; while the 84 Hz QPO corresponds either to $\ell = m = 6$ or to $\ell = 7$ and

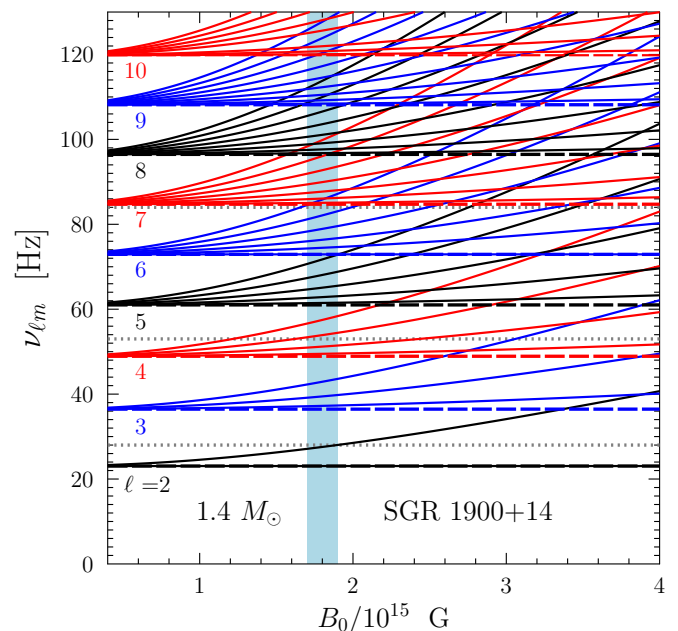


FIG. 8. Calculated frequencies of magneto-elastic oscillations versus B_0 for a $1.4 M_\odot$ magnetar model with the BSk21 EOS (from Fig. 1) are confronted with observations of QPOs from the giant flare of SGR 1900+14 (dotted lines). For illustration, the vertical darkened strip shows a possible range of B_0 for this particular toy model. See the text for details.

$m < 2$. The fourth QPO at 155 Hz is not plotted but it is evidently explained in this model.

Figure 9 is similar but designed to interpret much richer spectrum of QPOs observed from the hyperflare of SGR 1806–20. These QPOs cannot be explained assuming the $1.4M_{\odot}$ neutron star. A higher mass is required for the QPOs with lowest frequencies (e.g. Refs. [49, 50]): higher M reduces oscillation frequencies due to stronger gravitational redshift. In Fig. 9 we assume the $2.2M_{\odot}$ star. Choosing B_0 in the range $(2.7 \pm 0.12) \times 10^{15}$ G, we can be reasonably consistent with the data except for the triplet of QPOs with lowest frequencies (17, 18 and 21 Hz). It is not explained by our particular model, but can be easily attributed to deviations from the idealized $\mathbf{B}(\mathbf{r})$ configuration, given by Eqs. (21) and (29).

These exercises demonstrate once more that including the Zeeman splitting greatly affects interpretation of observed QPOs. In fact, it is sufficient to focus on explaining low frequency oscillations ($\nu \lesssim 100$ Hz), because the region of higher frequencies will be densely covered by Zeeman structures anyway. All low-frequency oscillations belong to fundamental modes which consideration is especially simple.

The model of toroidal magnetic fields studied above is the simplest one. Because of that we can formulate additional self-similarity rules, specific for this particular model. One needs only two numbers, $\nu_{\mu 0}$ and ν_{B0*} , to construct the FOPT oscillation frequencies, given by Eq. (31). To interpret the QPOs from one flare of a given SGR, it would be highly unreasonable to fix the neutron

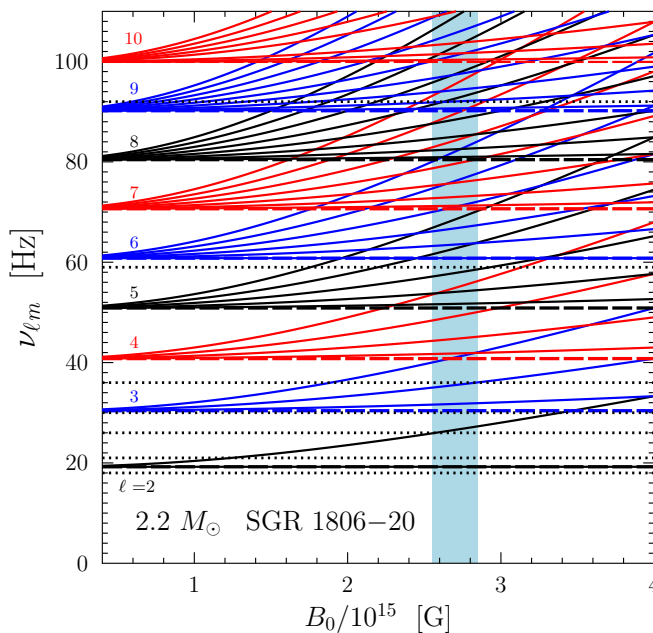


FIG. 9. Same as in Fig. 8 but employing the $2.2M_{\odot}$ neutron star model for explaining QPOs observed from the hyperflare of SGR 1806–20.

star model. It would be more profitable to consider $\nu_{\mu 0}$ and the product $(\nu_{B0*}B_*)$ as two independent fit parameters and try to find reliable best fits. In case of success, at the next step one can analyse these two best fit values with the hope to understand which neutron star and magnetic field parameters are physically sound. Because the fit gives the product $(\nu_{B0*}B_*)$, there appears internal ambiguity of the interpretation: one and the same value of the product will correspond to a family of different magnetic strengths B_0 and geometries, as well as different parameters of magnetar crust.

Let us remark that in Ref. [49, 50] we have studied similar magneto-elastic oscillations of magnetars using FOPT but assuming purely dipole magnetic field in the crust. Those results can be sensitive to a leakage of Alfvén perturbations outside the crust that was neglected. Nevertheless, the calculated spectra of magneto-elastic oscillations with account of the Zeeman splitting appeared rather similar to those obtained here (the largest difference was that the magnetic frequency ν_B depended on ℓ and did not vanish at $m = 0$). Illustrative attempts [49, 50] to interpret the same spectra of QPOs in the flaring SGR 1900+14 and SGR 1860–20 led to the same conclusions as here: (i) the SGR 1900+14 may have a typical neutron-star mass but the SGR 1860–20 needs to be massive; (ii) one needs magnetic fields $B \sim$ a few times of 10^{15} G in both SGRs, and the field of SGR 1806–20 is somewhat higher.

V. CONCLUSIONS

We have studied the Zeeman splitting of magneto-elastic oscillation frequencies of soft-gamma repeaters (SGRs), which are magnetars – neutron stars possessing very strong magnetic fields. The QPOs appear in occasional powerful flares of SGRs and can contain potentially important information on the physics of magnetar structure and evolution.

The Zeeman splitting of magnetar QPOs was predicted in Ref. [48]. Afterwards its study has been elaborated in two recent publications [49, 50].

In Sec. II we present the first-order perturbation theory (FOPT) of magneto-elastic oscillations localized in the magnetar crust, assuming axial symmetry of the crustal magnetic field $\mathbf{B}(\mathbf{r})$ and the presence of both, poloidal and toroidal, field components.

In Sec. III we apply these results for studying magneto-elastic oscillations in the presence of purely toroidal magnetic field, which forbids propagation of Alfvén perturbations outside the crust. The toroidal field is taken in the form (21). We describe amazing simplicity of the spectrum of fundamental oscillations (without radial nodes) and checked the validity of FOPT calculations using a restricted variational method. We analyse ranges of frequencies densely covered by numerous Zeeman components; at higher frequencies these ranges occur in lower magnetic fields. These results are in good qualitative

agreement with those obtained previously [49, 50] for dipole magnetic fields in the magnetar crust. In addition, we study, for the first time, the effects of magnetic fields on subsets of fine-structure components of ordinary oscillations (with radial nodes). Their Zeeman splitting creates additional frequency ranges densely filled with Zeeman structures.

Our calculations are mostly performed for the $1.4M_{\odot}$ magnetar model with the BSk21 EOS (Table I) but the self-similarity relations [26] allow us to extend the results to wider range of neutron star masses and describe oscillation spectra of numerous modes by a very limited amount of constants (Tables I and II). Similar description can be done for other EOSs.

Our schematic analysis of QPOs observed during the giant flare of SGR 1900+14 and the hyperflare of SGR 1806–20 supports previous conclusions [48–50] that the Zeeman effect is very important for a proper interpretation of the data. The main focus should be on low-frequency QPOs ($\nu \lesssim 150$ Hz) which can be interpreted as produced by fundamental magneto-acoustic oscillations at not too high magnetic fields $B \lesssim 3 \times 10^{15}$ G. Higher frequency QPOs fall in the range of frequencies densely covered by Zeeman structures even at lower B . The presented theory can identify them but the identification will be highly ambiguous.

On the other hand, we should state that neither theory nor observations are ready for the detailed analysis. The status of observations is outlined in Sec. IV. It has to be clarified. The present version of the theory can be improved in many ways. It would be more realistic to consider the magnetar’s magnetic field as a combination of toroidal and poloidal components (Sec. II). In such studies, one needs to go beyond the FOPT, analyse quasi-crossings of different modes and propagation of Alfvén perturbations outside the neutron star crust (Sec. II F). It is also desirable to solve the whole problem in full GR.

Let us stress again that the present calculations are performed for one EOS of neutron star matter and standard microphysics of the crust. One can vary the EOS and crustal microphysics, including different models of shear modulus, possible nuclear pasta layers at the crust bottom and nucleon superfluidity there, as discussed, for instance, in Sec. IV and in Refs. [26, 49]. This will af-

fect the interpretation of QPOs at the stage of accurate quantitative analysis.

Combining our results with the formalism of solving the Alfvén wave problem (Sec. II F) seems most important. Assuming a purely toroidal magnetic field localized in the crust, we artificially avoided it in this paper, but the step is inevitable. In more realistic cases, Alfvénic perturbations propagate into the stellar core, interact with the Alfvénic perturbations available there. This can affect crust-core coupling, damping of magneto-elastic oscillations and loss of their coherence. As a result, magnetar QPOs will depend on the structure, composition and microphysics of the entire star (particularly, on nucleon superfluidity and magnetic field geometry in the core) in a complicated way. As mentioned in Sec. II F, this effect has been studied in numerous publications. Unfortunately, all of them have been restricted by axially symmetric perturbations, while we stress the importance of axially asymmetric perturbations and suggest to elaborate the Alfvénic wave problem accordingly. Such elaboration would require a lot of efforts.

In addition, let us mention the long-standing problem of QPO formation, meaning detailed mechanism for transforming oscillations of surface neutron-star layers into observable QPOs. The problem seems important and feasible but remains unsolved.

Finally, we note that by demonstrating Zeeman splitting of oscillations on macroscopic (stellar) level, a magnetar behaves like a microscopic quantum object, resembling one giant atomic nucleus, just as Lev Landau envisioned a neutron star [56] in the very beginning of 1930s (see Ref. [57] for details).

ACKNOWLEDGMENTS

We are indebted to the anonymous referee for many useful remarks and critical comments. DY is grateful to M. E. Gusakov and E. M. Kantor for encouraging to study toroidal magnetic fields localized in the crust. The work was supported by the Russian Science Foundation, grant number 24-12-00320.

[1] S. L. Shapiro and S. A. Teukolsky, *Black holes, white dwarfs, and neutron stars: The physics of compact objects* (Wiley-Interscience, New York, 1983).
 [2] P. Haensel, A. Y. Potekhin, and D. G. Yakovlev, *Neutron Stars. 1. Equation of State and Structure* (Springer, New York, 2007).
 [3] V. M. Kaspi and A. M. Beloborodov, Magnetars, *Ann. Rev. Astron. Astrophys.* **55**, 261 (2017), arXiv:1703.00068 [astro-ph].
 [4] R. C. Duncan, Global Seismic Oscillations in Soft Gamma Repeaters, *Astrophys. J. Lett.* **498**, L45 (1998),

arXiv:astro-ph/9803060 [astro-ph].
 [5] G. L. Israel, T. Belloni, L. Stella, Y. Rephaeli, D. E. Gruber, P. Casella, S. Dall’Osso, N. Rea, M. Persic, and R. E. Rothschild, The Discovery of Rapid X-Ray Oscillations in the Tail of the SGR 1806-20 Hyperflare, *Astrophys. J. Lett.* **628**, L53 (2005), arXiv:astro-ph/0505255 [astro-ph].
 [6] T. E. Strohmayer and A. L. Watts, Discovery of Fast X-Ray Oscillations during the 1998 Giant Flare from SGR 1900+14, *Astrophys. J. Lett.* **632**, L111 (2005), arXiv:astro-ph/0508206 [astro-ph].

- [7] A. L. Watts and T. E. Strohmayer, Detection with RHESSI of High-Frequency X-Ray Oscillations in the Tail of the 2004 Hyperflare from SGR 1806-20, *Astrophys. J. Lett.* **637**, L117 (2006), arXiv:astro-ph/0512630 [astro-ph].
- [8] V. Hambaryan, R. Neuhäuser, and K. D. Kokkotas, Bayesian timing analysis of giant flare of SGR 180620 by RXTE PCA, *Astron. Astrophys.* **528**, A45 (2011), arXiv:1012.5654 [astro-ph.SR].
- [9] D. Huppenkothen, L. M. Heil, A. L. Watts, and E. Göğüş, Quasi-periodic Oscillations in Short Recurring Bursts of Magnetars SGR 1806-20 and SGR 1900+14 Observed with RXTE, *Astrophys. J.* **795**, 114 (2014), arXiv:1409.7642 [astro-ph.HE].
- [10] D. Huppenkothen, C. D'Angelo, A. L. Watts, L. Heil, M. van der Klis, A. J. van der Horst, C. Kouveliotou, M. G. Baring, E. Göğüş, J. Granot, Y. Kaneko, L. Lin, A. von Kienlin, and G. Younes, Quasi-periodic Oscillations in Short Recurring Bursts of the Soft Gamma Repeater J1550-5418, *Astrophys. J.* **787**, 128 (2014), arXiv:1404.2756 [astro-ph.HE].
- [11] D. Pumpe, M. Gabler, T. Steininger, and T. A. Enßlin, Search for quasi-periodic signals in magnetar giant flares. Bayesian inspection of SGR 1806-20 and SGR 1900+14, *Astron. Astrophys.* **610**, A61 (2018), arXiv:1708.05702 [astro-ph.HE].
- [12] C. J. Hansen and D. F. Cioffi, Torsional oscillations in neutron star crusts, *Astrophys. J.* **238**, 740 (1980).
- [13] B. L. Schumaker and K. S. Thorne, Torsional oscillations of neutron stars, *Mon. Not. R. Astron. Soc.* **203**, 457 (1983).
- [14] P. N. McDermott, H. M. van Horn, and C. J. Hansen, Nonradial Oscillations of Neutron Stars, *Astrophys. J.* **325**, 725 (1988).
- [15] L. Samuelsson and N. Andersson, Neutron star asteroseismology. Axial crust oscillations in the Cowling approximation, *Mon. Not. R. Astron. Soc.* **374**, 256 (2007), arXiv:astro-ph/0609265 [astro-ph].
- [16] N. Andersson, K. Glampedakis, and L. Samuelsson, Superfluid signatures in magnetar seismology, *Mon. Not. R. Astron. Soc.* **396**, 894 (2009), arXiv:0812.2417 [astro-ph].
- [17] H. Sotani, K. Nakazato, K. Iida, and K. Oyamatsu, Probing the Equation of State of Nuclear Matter via Neutron Star Asteroseismology, *Phys. Rev. Lett.* **108**, 201101 (2012), arXiv:1202.6242 [astro-ph.HE].
- [18] H. Sotani, K. Nakazato, K. Iida, and K. Oyamatsu, Effect of superfluidity on neutron star oscillations, *Mon. Not. R. Astron. Soc.* **428**, L21 (2013), arXiv:1210.0955 [astro-ph.HE].
- [19] H. Sotani, K. Nakazato, K. Iida, and K. Oyamatsu, Possible constraints on the density dependence of the nuclear symmetry energy from quasi-periodic oscillations in soft gamma repeaters, *Mon. Not. R. Astron. Soc.* **434**, 2060 (2013), arXiv:1303.4500 [astro-ph.HE].
- [20] H. Sotani, Empirical formula of crustal torsional oscillations, *Phys. Rev. D* **93**, 044059 (2016), arXiv:1602.04558 [astro-ph.HE].
- [21] H. Sotani, K. Iida, and K. Oyamatsu, Probing nuclear bubble structure via neutron star asteroseismology, *Mon. Not. R. Astron. Soc.* **464**, 3101 (2017), arXiv:1609.01802 [astro-ph.HE].
- [22] H. Sotani, K. Iida, and K. Oyamatsu, Probing crustal structures from neutron star compactness, *Mon. Not. R. Astron. Soc.* **470**, 4397 (2017), arXiv:1706.04736 [astro-ph.HE].
- [23] H. Sotani, K. Iida, and K. Oyamatsu, Constraints on the nuclear equation of state and the neutron star structure from crustal torsional oscillations, *Mon. Not. R. Astron. Soc.* **479**, 4735 (2018), arXiv:1807.00528 [astro-ph.HE].
- [24] H. Sotani, K. Iida, and K. Oyamatsu, Astrophysical implications of double-layer torsional oscillations in a neutron star crust as a lasagna sandwich, *Mon. Not. R. Astron. Soc.* **489**, 3022 (2019), arXiv:1906.06999 [astro-ph.HE].
- [25] A. A. Kozhberov and D. G. Yakovlev, Deformed crystals and torsional oscillations of neutron star crust, *Mon. Not. R. Astron. Soc.* **498**, 5149 (2020), arXiv:2009.04952 [astro-ph.HE].
- [26] D. G. Yakovlev, Self-similarity relations for torsional oscillations of neutron stars, *Mon. Not. R. Astron. Soc.* **518**, 1148 (2023), arXiv:2210.02931 [astro-ph.SR].
- [27] Y. Levin, QPOs during magnetar flares are not driven by mechanical normal modes of the crust, *Mon. Not. R. Astron. Soc.* **368**, L35 (2006), arXiv:astro-ph/0601020 [astro-ph].
- [28] K. Glampedakis, L. Samuelsson, and N. Andersson, Elastic or magnetic? A toy model for global magnetar oscillations with implications for quasi-periodic oscillations during flares, *Mon. Not. R. Astron. Soc.* **371**, L74 (2006), arXiv:astro-ph/0605461 [astro-ph].
- [29] H. Sotani, K. D. Kokkotas, and N. Stergioulas, Torsional oscillations of relativistic stars with dipole magnetic fields, *Mon. Not. R. Astron. Soc.* **375**, 261 (2007), arXiv:astro-ph/0608626 [astro-ph].
- [30] Y. Levin, On the theory of magnetar QPOs, *Mon. Not. R. Astron. Soc.* **377**, 159 (2007), arXiv:astro-ph/0612725 [astro-ph].
- [31] H. Sotani, K. D. Kokkotas, and N. Stergioulas, Alfvén quasi-periodic oscillations in magnetars, *Mon. Not. R. Astron. Soc.* **385**, L5 (2008), arXiv:0710.1113 [astro-ph].
- [32] U. Lee, Axisymmetric toroidal modes of magnetized neutron stars, *Mon. Not. R. Astron. Soc.* **385**, 2069 (2008), arXiv:0710.4986 [astro-ph].
- [33] A. Colaiuda, H. Beyer, and K. D. Kokkotas, On the quasi-periodic oscillations in magnetars, *Mon. Not. R. Astron. Soc.* **396**, 1441 (2009), arXiv:0902.1401 [astro-ph.HE].
- [34] P. Cerdá-Durán, N. Stergioulas, and J. A. Font, Alfvén QPOs in magnetars in the anelastic approximation, *Mon. Not. R. Astron. Soc.* **397**, 1607 (2009), arXiv:0902.1472 [astro-ph.HE].
- [35] M. Gabler, P. Cerdá Durán, J. A. Font, E. Müller, and N. Stergioulas, Magneto-elastic oscillations and the damping of crustal shear modes in magnetars, *Mon. Not. R. Astron. Soc.* **410**, L37 (2011), arXiv:1007.0856 [astro-ph.HE].
- [36] M. van Hoven and Y. Levin, Magnetar oscillations - I. Strongly coupled dynamics of the crust and the core, *Mon. Not. R. Astron. Soc.* **410**, 1036 (2011), arXiv:1006.0348 [astro-ph.HE].
- [37] A. Colaiuda and K. D. Kokkotas, Magnetar oscillations in the presence of a crust, *Mon. Not. R. Astron. Soc.* **414**, 3014 (2011), arXiv:1012.3103 [gr-qc].
- [38] M. van Hoven and Y. Levin, Magnetar oscillations - II. Spectral method, *Mon. Not. R. Astron. Soc.* **420**, 3035 (2012), arXiv:1110.2107 [astro-ph.HE].
- [39] M. Gabler, P. Cerdá-Durán, N. Stergioulas, J. A. Font, and E. Müller, Magnetoelastic oscillations of neutron

- stars with dipolar magnetic fields, *Mon. Not. R. Astron. Soc.* **421**, 2054 (2012), arXiv:1109.6233 [astro-ph.HE].
- [40] A. Colaiuda and K. D. Kokkotas, Coupled polar-axial magnetar oscillations, *Mon. Not. R. Astron. Soc.* **423**, 811 (2012), arXiv:1112.3561 [astro-ph.HE].
- [41] M. Gabler, P. Cerdá-Durán, J. A. Font, E. Müller, and N. Stergioulas, Magneto-elastic oscillations of neutron stars: exploring different magnetic field configurations, *Mon. Not. R. Astron. Soc.* **430**, 1811 (2013), arXiv:1208.6443 [astro-ph.SR].
- [42] M. Gabler, P. Cerdá-Durán, N. Stergioulas, J. A. Font, and E. Müller, Imprints of Superfluidity on Magnetoelastic Quasiperiodic Oscillations of Soft Gamma-Ray Repeaters, *Phys. Rev. Lett.* **111**, 211102 (2013), arXiv:1304.3566 [astro-ph.HE].
- [43] A. Passamonti and S. K. Lander, Quasi-periodic oscillations in superfluid magnetars, *Mon. Not. R. Astron. Soc.* **438**, 156 (2014), arXiv:1307.3210 [astro-ph.SR].
- [44] B. Link and C. A. van Eysden, Torsional Oscillations of a Magnetar with a Tangled Magnetic Field, *Astrophys. J. Lett.* **823**, L1 (2016), arXiv:1604.02372 [astro-ph.HE].
- [45] M. Gabler, P. Cerdá-Durán, N. Stergioulas, J. A. Font, and E. Müller, Coherent magneto-elastic oscillations in superfluid magnetars, *Mon. Not. R. Astron. Soc.* **460**, 4242 (2016), arXiv:1605.07638 [astro-ph.HE].
- [46] M. Gabler, P. Cerdá-Durán, N. Stergioulas, J. A. Font, and E. Müller, Constraining properties of high-density matter in neutron stars with magneto-elastic oscillations, *Mon. Not. R. Astron. Soc.* **476**, 4199 (2018), arXiv:1710.02334 [astro-ph.HE].
- [47] L. Cheung, L.-M. Lin, and N. Chamel, Torsional oscillations of magnetized neutron stars: Impacts of Landau-Rabi quantization of electron motion, *Phys. Rev. D* **110**, 083021 (2024), arXiv:2312.05676 [astro-ph.HE].
- [48] R. Shaisultanov and D. Eichler, What Magnetar Seismology Can Teach Us About Magnetic Fields, *Astrophys. J. Lett.* **702**, L23 (2009), arXiv:0903.3319 [astro-ph.HE].
- [49] D. Yakovlev, Zeeman Splitting of Torsional Oscillation Frequencies of Magnetars, *Universe* **9**, 504 (2023), arXiv:2312.10022 [astro-ph.HE].
- [50] D. G. Yakovlev, Powerful flares and magneto-elastic oscillations of magnetars, *Zh. Exp. Teor. Fiz.* **166**, 121 (2024), arXiv:2409.11178 [astro-ph].
- [51] G. Arfken, *Mathematical Methods for Physicists* (Academic Press, New York, 1966).
- [52] L. D. Landau and E. M. Lifshitz, *Quantum Mechanics* (Oxford: Pergamon Press, 1976).
- [53] D. N. Aguilera, J. A. Pons, and J. A. Miralles, 2D Cooling of magnetized neutron stars, *Astron. Astrophys.* **486**, 255 (2008), arXiv:0710.0854 [astro-ph].
- [54] A. Y. Potekhin, A. F. Fantina, N. Chamel, J. M. Pearson, and S. Goriely, Analytical representations of unified equations of state for neutron-star matter, *Astron. Astrophys.* **560**, A48 (2013), arXiv:1310.0049 [astro-ph.SR].
- [55] S. Ogata and S. Ichimaru, First-principles calculations of shear moduli for Monte Carlo-simulated Coulomb solids, *Phys. Rev. A* **42**, 4867 (1990).
- [56] L. D. Landau, To the Stars theory, *Phys. Zs. Sowjet* **1**, 285 (1932).
- [57] D. G. Yakovlev, P. Haensel, G. Baym, and C. Pethick, Lev Landau and the concept of neutron stars, *Physics Uspekhi* **56**, 289-295 (2013), arXiv:1210.0682 [physics.hist-ph].